Cloud Publications
International Journal of Advanced Remote Sensing and GIS
2017, Volume 6, Issue 1, pp. 2204-2222
ISSN 2320 – 0243, Crossref: 10.23953/cloud.ijarsg.274

Research Article

Land Surface Temperature Extracts for Peri-Urban Heat and Rural Cool Troughs in Ghana

Divine Odame Appiah[1], Eric Kwabena Forkuo[2] and John Tiah Bugri[3]

[1]Department of Geography and Rural Development, Kwame Nkrumah University of Science and Technology, (KNUST) Kumasi, Ghana
[2]Department of Geomatic Engineering, Kwame Nkrumah University of Science and Technology, (KNUST) Kumasi, Ghana
[3]Department of Land Economy, Kwame Nkrumah University of Science and Technology, (KNUST) Kumasi, Ghana

Publication Date: 10 June 2017

DOI: https://doi.org/10.23953/cloud.ijarsg.274

Abstract The objective of this paper is to analyze the land surface temperatures (LST) derived from three satellite images as a proxy for urban heat island potential, through a peri-urban heat troughs (PuHT) to rural cool troughs (RuCT) continuum, concepts largely overlooked in the literature, in the Bosomtwe district of the Ashanti region of Ghana. Four Landsat satellite images from 2002, 2008 Enhanced Thematic Mapper+ (ETM+) and 2014 Landsat 8 Operational Land Imager and Thermal Infrared Sensor (OLI/TIRS) were geo-referenced and processed for classification using the maximum likelihood classifier algorithm in ERDAS Imagine 13. Land Use and Land Cover (LULC) transition analysis was performed in ArcMap for ArcGIS 10.2. Results indicate that, in order of importance, recent fallows and grasslands along with built up/bare land and concrete surfaces have been increasing in terms of coverage. A corresponding surface reflectance translated into LST values ranging between a minimum of 24ºC (297K) to a maximum of 53ºC (326K). Changing LULC types correlated with the land surface temperature fluxes, creating the RuCT and PuHT. This result explains the relatively substantial peri-urban land use dynamics in the district. Future studies should develop threshold values for RuCT and PuHT temperatures.
Keywords *Peri-urban heat trough (PuHT); Rural cool trough (RuCT); Land Surface Temperature (LST); Land Use Land Cover (LULC); Bosomtwe; Ghana*

1. Introduction

Land surface characteristics determine the amount of energy that is absorbed and emitted. The reflectance and emission properties of land surface features also determine the albedo that defines the percentage reflectance of solar energy from the earth surface (Ahrens, 2005). As a proxy for calculating the degree of hotness or coldness of the land surface, many researchers have used thermal infrared (TIR) satellite remote sensing to estimate land surface reflectance properties to extract surface temperature and moisture for climatic analysis (Rajeshwari et al., 2014; Liu and Zhang, 2011 and Srivastava et al., 2010). Land use and land cover (LULC) dynamics influence the ability of land surfaces to absorb or reflect solar radiation in varying proportions.

In furtherance of handling LULC dynamics, previous studies have indicated that depending on the type of LULC obtained, it could be possible to extract surface moisture and temperature characteristics from LULC maps generated from Advanced Space-borne Thermal Emission and Reflection Radiometer (ASTER), Landsat, MODIS and others (Ahrens, 2005; Liu and Zhang, 2011 and Srivastava et al., 2010). Accordingly, the energy emitted by the LULC mosaic as indicated by its surface energy fluxes and atmospheric conditions, aids in determining the varying energy fluxes of land surfaces (Vlassova et al., 2014).

In peri-urban landscapes, the complex mixture of settlement and vegetation exhibit different energy fluxes. This phenomenon determines the amount of surface temperature that can be sensed and recorded. In a study by Sobrino et al. (2004), the relationship between vegetation and land surface temperature was established by correlating normalized difference vegetation indices (NDVIs) with the temperature profiles of land use classes. Widyasamratri et al. (2013) found that there are limitations in accessing and using air temperature of an area to represent actual temperature characteristics in investigations of urban heat islands (UHIs) and similar phenomena. This limitation could be reduced through the use of NDVIs and correlated against estimated land surface temperature (LST) as proximate analysis for climate change analysis (Mbithi, nd; Weng, 2004; Weng, 2001).

As a result, the data obtained from NDVIs are typically used to determine the effectual land surface radiating temperature that affect surface energy and vapor fluxes interacting with the atmosphere (Yuan and Bauer, 2007). According to Vlassova et al. (2014), LULC dynamics reflects the surface temperature characteristics, which serve as surrogates for documenting climate change using proximate variables such as temperature and rainfall. This data reinforces the Intergovernmental Panel on Climate Change Fourth Assessment Report (IPCCAR4) and cited in (Meehl et al., 2007), that projected mean annual precipitation will demonstrate increasing and decreasing trends in high northern latitudes of the tropics and the subtropics, respectively.

LST estimates have been conducted by Widyasamratri et al. (2013) to measure the rate and intensity of urbanization in Jakarta, Indonesia. From that study a relationship between urbanization and UHI was established for the city. Modification of LULC types usually results in altered land surface temperatures (Asmat et al., 2016). The peri-urban mosaic consists of a complex mixture of rural and urban LULC classes, which clearly exhibits diverse surface reflectance and emissivity configurations (Rajeshwari and Mani, 2014). Using remote sensing and geographic information system (GIS) techniques; it is easier to estimate the surface temperature profiles of these peri-urban LULCs.

Research conducted by Voogt and Oke (2003), indicated that higher temperature values are associated with urban rock and built-up areas, while lower temperatures exemplify rural landscapes. These sharp temperature contrasts have aided in the measurement of environmental reflectance propensities of the various LULC types, which exhibit localized effects while contributing to regional and global heat budgets in the long term (Joshi and Bhatt, 2012).

Again, beyond the statistical assessment of land use and land cover changes (LULCCs) obtained from classified satellite images, LSTs correspond to certain land use classes that can be derived from the TIR band of the satellite image (Mbithi et al., nd; Urban et al., 2003). These results may portray the latent and sensible heat energy fluxes exhibited by the LULCC dynamics. From a temporal dimension, it is plausible to mimic the dynamics of particular climatic variables and to eventually, project some variability or even changes in local to regional climates (Blake et al., 2011; Iino and Hoyano, 1996 and Lipton and Ward, 2000). Satellite remote sensing with a GIS framework has been used to study UHI differentials (Quattrochi et al., 2000). These techniques were employed to juxtapose LULC variations with LST anomalies extracted from satellite images (Ambinakudige, 2011).

As an alternative to the analysis of LST as surrogate to climate change, the use of down-scaled Regional and Global Climate Models (RGCMs) has facilitated to an appreciable extent, the forecasting of future climate scenarios in many instances (Thomas, 2008). The RGCM data, with typically low spatial and temporal resolution of several degrees, usually have error-laden results to preclude their use in accurately simulating present-day climate (Bonan et al., 2002). In employing RCMs in regional climate simulations, higher spatial resolution data usually performs sufficiently for providing adequate scientific insights into regional climate change analysis (Khang et al., 2009). Some of these models, such as the CCSM3 2005 of the US National Center for atmospheric Research (NCAR) and the UKMO/HadGEM1 2004 of the United Kingdom, have high regional climate simulation capabilities (Khang et al., 2009).

In placing the current study in the context of conventional methods and procedures, the Bosomtwe district, with an area of 330km^2, is arguably too small to significantly influence local to regional climatic conditions in terms of rainfall and temperature variables if model downscaling methods are used. LULC dynamics extracted from satellite images prescribe different spatio-temporal changing dynamics of the LULC types, with their possible effects on land surface reflectance. This assumption underpins the use of LST extraction from satellite images and juxtaposing that data with the LULC types derived from the LULCC patterns observed in the Bosomtwe study area.

2. Theoretical Basis of Land Surface Temperature (LST) extraction Algorithms

In a study by Dousset and Gourmelon (Dousset, and Gourmelon, 2003) and cited by Chen et al. (2006), there is a methodological potential for establishing relationships between urban LST and LULC categories using satellite multi-sensor data. From this analysis Chen et al. (2006), a correlation between urban land uses, along with nighttime and daytime average LST profiles, was established.

According to Rajeshwari and Mani (2014), several algorithms have been developed and employed in the estimation of LST. Some of the frequently-used algorithms are Split-Window (SW), Sobrino, Mao, Dual-Angle, and Sob-Mao. Most studies focused on urban areas and arid and semi-arid regions. In many of these studies, a single thermal band was used. These approaches were used to extract the LSTs from ASTER and MODIS data (Sobrino et al., 2003). Again, Jiménez-Muñoz et al., (2006) and cited in Srivastava et al. (2010), used an NDVI-based approach to derive surface emissivity over agricultural areas using ASTER images. Further, Coll et al., (2005) had also compared LST estimates between ASTER and MODIS images in their study.

Inverting the radiative transfer equation (RTE) is the most appropriate process for retrieving LST from a single-channel identified in the TIR region, just like a Landsat image (Cristobal et al., 2009). This is expressed as per the wavelength of the spectrum sensed as follows:

$$L_{sensor,\lambda} = \left[\varepsilon_\lambda B_\lambda (T_s) + (1-\varepsilon_\lambda) L\downarrow_{atm,\lambda}\right]\tau_\lambda + L\uparrow_{atm,\lambda} \quad (1)$$

Where L_{sensor} is the top of atmospheric (TOA) radiance, $\boldsymbol{\varepsilon}$ represents the surface emissivity, B_λ (T_s) is the black body radiance derived by the Planck's law and T_s is the LST. $L\downarrow_{atm,\lambda}$ is the downwelling atmospheric radiance, $\boldsymbol{\tau}$ is the total atmospheric transmissivity between the surface and the sensor, and $L\uparrow_{atm,\lambda}$ is the upwelling atmospheric radiance. It should be noted that Eqn. (1) depends on the wavelength used and also on the observation orientation of sensor platform, although for Landsat, the nadir view offers better outcomes.

The atmospheric parameters τ, $L\downarrow_{atm,\lambda}$ and $L\uparrow_{atm,\lambda}$ are estimated from *in situ* radio-sounding operated on radiative transfer codes such as MODTRAN [31]. Therefore, from Eqn. (2), T_s is derived by using

the inversion of Planck's law. A further inversion of Eqn. (2) is used to correct atmospheric as well as emissivity effects on the measured data by the sensor. The crucial challenge of this method, however, is the need for radio-sounding to be simultaneously launched with the satellite tracking system (Cristobal et al., 2009).

Radiances are in W m^{-2} sr^{-1} μm^{-1} and wavelength in *μm*; the B term is Planck's law, expressed as follows:

$$B(\lambda, T_s) = \frac{c_1 \lambda^{-5}}{\exp\left(\frac{c_2}{\lambda T_s}\right) - 1} \qquad (2)$$

Where c_1 and c_2 are Planck's radiation constants, having values of 1.19104 x 10^8 Wμm^4 m^{-2} sr^{-1} and 1.43877 x 10^4 μm K, respectively, while T_s and λ are the surface temperature in K and thermal bands wavelength in *μm*. Accordingly, it is pertinent to note that the spectral magnitudes should be integrated over a band pass, in the case of Landsat sensors. This coheres with the work of Jiménez-Muñoz et al. (2013), which employed radiative transfer equation on a single-channel to extract LST.

2.1. The Concepts of Peri-Urban Heat Trough (PuHT) and Rural Cool Trough (RuCT)

Many studies have concentrated attention on the generation of temperature profiles to measure UHI fluxes (Liu et al., 2011; Srivastava et al., 2010; Mbithi et al., nd; Weng et al., 2004 and (Weng, 2001). UHI and its impact on rainfall may have been modified by local climate change; however, the quantitative dimensions are yet to be unraveled (Blake, 2011). Most of these studies have not considered explicitly the effects of PuHT systems becoming potential peri-urban heat islands in transition from the RuCT, into becoming ultimately, the so-called urban heat islands (UHIs) (Liu et al., 2011).

Both PuHT and RuCT concepts refer to the concentration of surface up-welling heat energy fluxes that can be sensed as evidence of changing land use patterns in peri-urban and rural landscapes, respectively. These sensible heat fluxes result from the modification and conversion of vegetative and rural LULC types to considerable built-up land use types (Carnahan and Larson, 1990; Baylis et al., 1999). These correlate with moderate to extreme LULC characteristics of the peri-urban and urban landscape, with varying LST configuration (Srivastava et al., 2010). PuHT could be described as the incipient stages of UHIs; the former, however, having a relatively wider geo-spatial dimension in comparison to the latter.

These surface temperature profiles occur due to the progressive increase in urbanization of the rural landscape. As a result, peri-urbanization processes ensue to alter the previously rural land surface characteristics into peri-urban and urban land surface configurations. The land surface characteristics, therefore, result in the RuCT, moderate PuHT and an ultimate UHI core in continuum. The resultant is a LST gradient that develops along the rural to urban lands surface continuum.

Previous studies on land surface heating fluxes have largely focused on core UHIs as surrogates of extraction urban climates (Srivastava et al., 2010). The literature, however, remains sparse on the potentially significant role of PUAs in fuelling the ultimate heat island system. This study proposes that, considering the relative rapidity with which rural landscapes are being converted into peri-urban land uses, with surface reflectance transforming into built-up and paved land uses, it is imperative to analyze the connections between RuCTs and the PuHT systems as potentially full-fledged heat island cell areas. The objective of this paper is to analyze the LST derived from three satellite images, as a

proxy for the creation of potential UHIs through PuHT and RuCT continuum, in the Bosomtwe district of the Ashanti region of Ghana. This paper discusses the omissions of LST transitions from the rural, with preponderance of vegetation, to the urban core with high built-up surfaces. It does so by relating the LULC dynamics of the Bosomtwe peri-urban district, to determine LST fluxes; typical of peri-urban areas. The introduction of the concepts of the RuCT and PuHT into the literature, give credence to the potential LST continuum profiles between the rural 'cool' and urban 'hot' areas, using the peri-urban areas as the transitional zones.

3. Materials and Methods

3.1. Profile of the study area

The study area lies within latitude 6º28'N—latitude 6º40'N and longitudes 1º20'W—longitude 1º37'W in the Ashanti region of Ghana. It has a land area of 330km^2, as seen in Figure 1. The largest Crater Lake in Ghana, Lake Bosomtwe, is located in the district. The area is characterized by a rolling topography which ranges between 500 and 1500m above sea level. The drainage patterns of rivers and streams of the district are dendritic and centripetal (Carnahan and Larson, 1990). Rivers that drain the basin include *oda, butu, siso, supan* and *adanbanwe*.

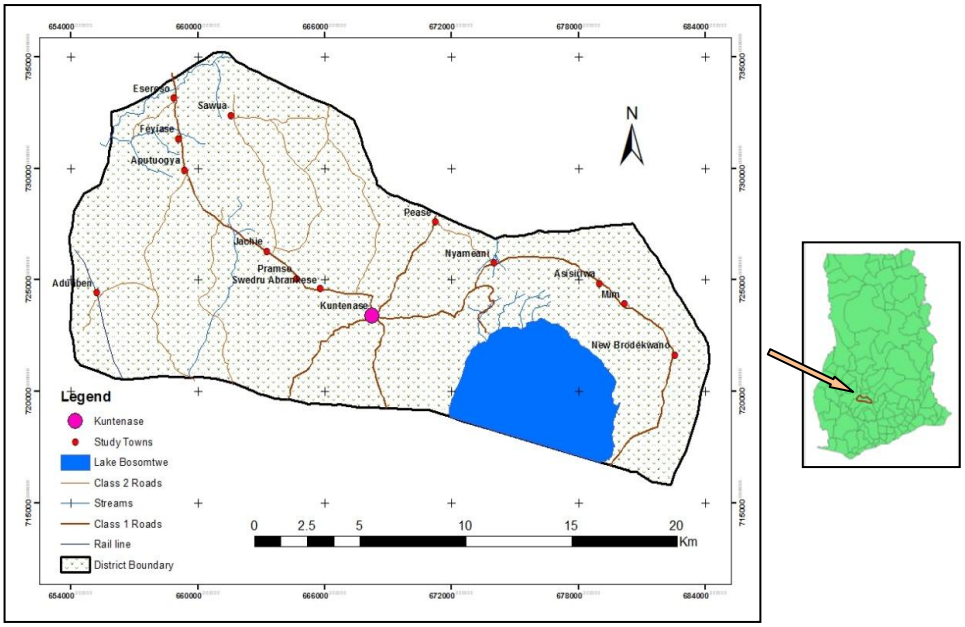

Figure 1: *Map of the Bosomtwe District showing the study communities in Ghana*

The district's rainfall regime is typical of the moist semi-deciduous forest zone of the country, showing two well-defined rainy seasons. The main rainy season occurs from March to July, while September to November constitutes the minor rainy season with an average annual rainfall of 1,400 mm. The mean monthly temperature is around 32°C with a relative humidity of up to 85%.

The district exhibits semi-deciduous forest vegetation characteristics, with different species of tropical trees with high economic value. The dominant tree species native to the district include: wawa *(Triplochiton scleroxylon),* mahogany *(Khaya ivorensis),* and onyina *(Ceiba pentandra)*. Through overharvesting, the original forest cover has been converted into secondary and grassland vegetation. Slash and burn agricultural methods as well as illegal gold mining activities are also responsible for the land and vegetation cover alterations.

The expansion of villages in the district is influenced by the proximity between the district and peripheral settlements of the greater Kumasi metropolitan area, the capital of the Ashanti region of Ghana. Increases in infrastructure, socioeconomic activities, and tourism have contributed to LULCCs in the district.

3.2 Data and Software

3.2.1 Sources of Data

Landsat 7 Enhanced Thematic Mapper (ETM), Landsat 7 Enhanced Thematic Mapper plus (ETM+), and Landsat 8 Operational Land Imager/Thermal Infrared sensor (OLI/TIRS) with a spatial resolution of 30m x 30m were used (see Table 1 and Figure 2(a-c)). The use of these images was informed by their availability and relative clarity in terms of cloud cover and other forms of instrument noise. The use of these three was based on their relative image quality which required minimal radiometric correction.

Table 1: *Satellite image characteristics*

Year	Satellite Sensor	Date acquired	Bands used
2002	Landsat 7 ETM	May 7	1,2,3,4,5,6
2008	Landsat 7 ETM+	February 16	1,2,3,4,5,6
2014	Landsat 8 OLI/TIS	January 8	2,3,4,5,10,11

Because of the coarser spatial resolution of Landsat TM/ETM/TIRS images at 30m x 30m, it was not methodologically expedient to downscale climatic variables from any regional climate model (RCM) for the analysis of climate change and variability to any appreciable extent in this study. It is therefore convenient to use another approach of extracting climate variability from the satellite image and comparing it with some air temperature point data (7), (11).

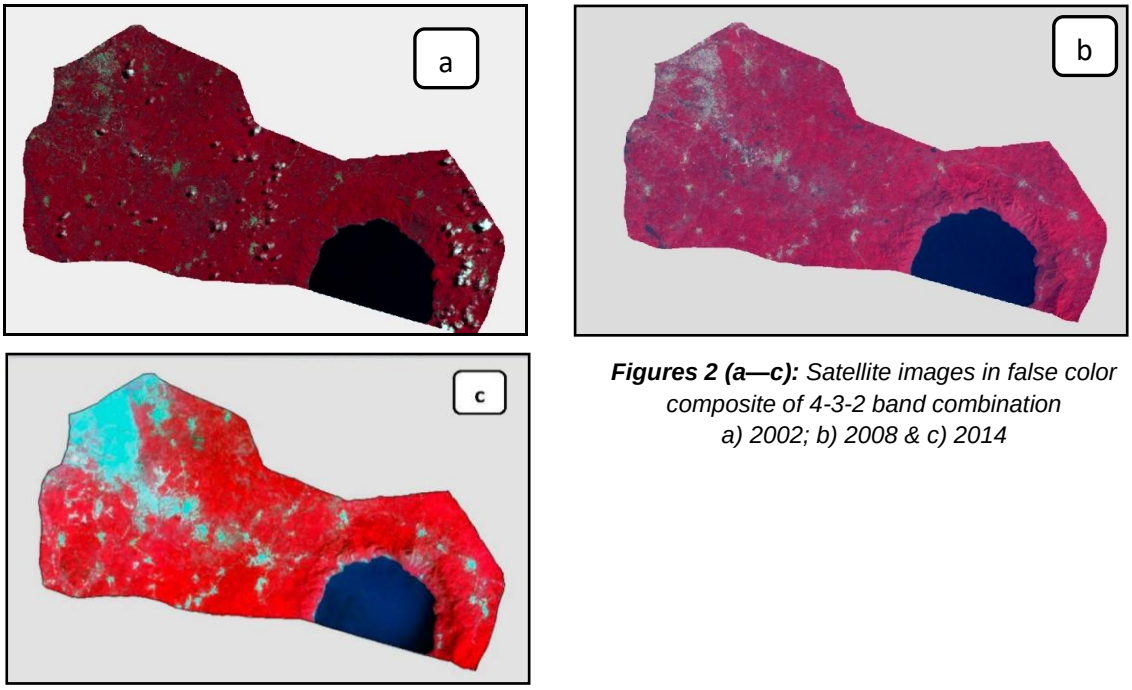

Figures 2 (a—c): *Satellite images in false color composite of 4-3-2 band combination*
a) 2002; b) 2008 & c) 2014

3.2.2 Software used

The Hexagon Geospatial ERDAS Imagine 13, ENVI 4.7, and ESRI's ArcGIS v.10.2 software were used for data analyses (Figure 3). The Garmin eTrex 20® Global Position System (GPS) receiver was used to randomly select 58 coordinates of selected LULC as ground control points (GCPs) during field work, at ±3m accuracy. These points were loaded and imputed into the remote sensing software to perform the accuracy checks on the image classification. The maximum likelihood classifier (MLC) algorithm was used, after satisfying the assumptions of image data normality.

The LULC classes were derived based on field experience and familiarity with the study area as well as their spectral characteristics. The LULC schema used was based on (Baylis et al., 1999) classes types identified as: dense forest (DF), low forest (LF), built-up/bare lands and concrete (BBC) surfaces, recent fallows and grassland (RFG) as well as water body (WB). Three criteria informed the selection of the images used: 1. The quality of the images with respect to the percentage of cloud cover and other image noise, 2. The years with considerable evidence of vegetation regeneration after the 1980s bush fires (due to prolonged drought conditions), and 3. The need to ascertain LULC trends over a 12-year period (which is considered long enough to detect and generate meaningful LULCCs).

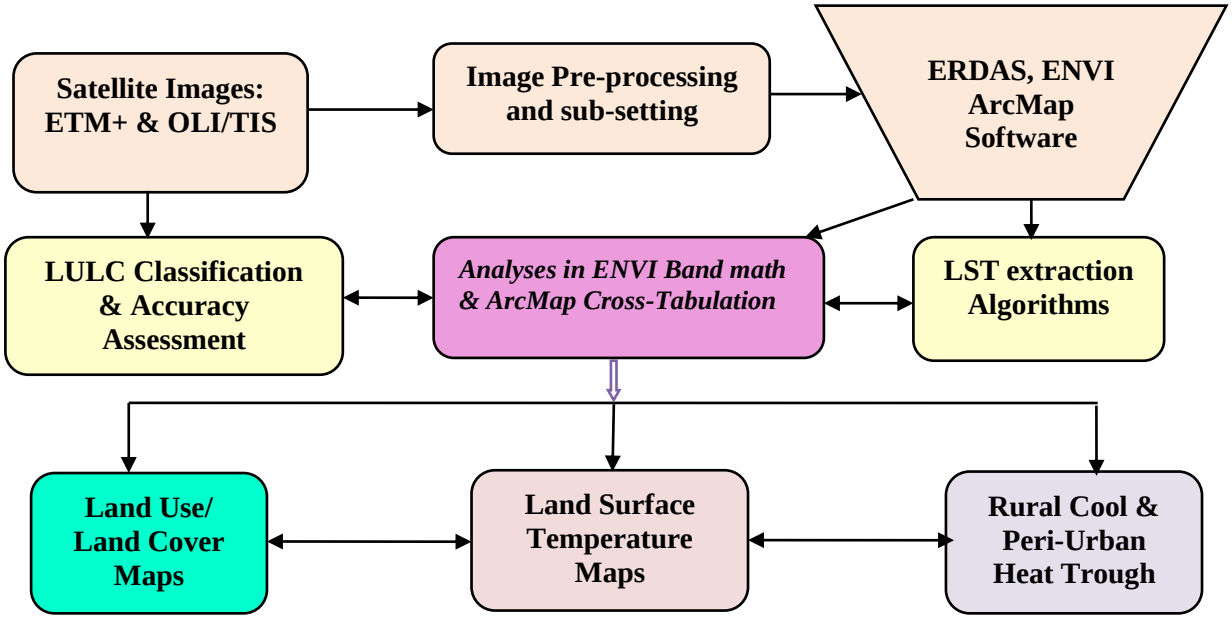

Figure 3: *Methodological flow chart of the LULC and LST extraction procedures*

3.2.3 Spectral Radiance Scaling Method

Conversion from digital numbers to top of atmosphere (TOA) radiance was performed using image meta data Kepner et al. (2000), in ENVI 4.7 software (Butt et al., 2015). In this regard, the formula to convert cell value as DN to cell value as radiance CV_{R1} for the three images, utilized the formula as follows:

$$CV_{RI} = \left(\frac{(L\max - L\min)}{QCALMax - QCAL\min} \right) X \left(QCAL - QCAL\min \right) + L\min \qquad (3)$$

Where CV_{RI} is cell value as radiance, QCAL is digital number, Lmin is spectral radiance scales to QCALmin, Lmax is spectral radiance scales to QCALmax, QCALmin is the minimum quantized calibrated pixel value (estimated as 1), and QCALmax is the maximum quantized calibrated pixel value (typically = 255) (Chander and Markham, 2003).

3.2.4. Apparent Brightness Temperature

The formula to convert radiance to temperature *without* atmospheric correction method was used in converting the radiance to temperature in Kelvin (Kepner et al., 2000). The apparent brightness temperature or at-sensor brightness temperature (T_b), was determined by applying blackbody principles, which is usually computed by means of Planck's law inversion using the Landsat image series USGS (2015), with the following simplified equation:

$$T_b = \frac{K_2}{\left(\frac{K_1 * \varepsilon}{CV_{R1}} + 1\right)} \tag{4}$$

Where, ε is the emissivity (*typically 0.95, and could as well be derived from NDVIs*). The K_1 and K_2 (K) (W m^{-2} sr^{-1} mm^{-1}), are calibration constants based on the Landsat thermal band configuration and CV_{R1} is the spectral radiance (W m^{-2} sr^{-1} mm^{-1}). In the case of Landsat 7, K_1 and K_2 are 666.09 and 1282.71, respectively. With Landsat 8, the K_1 and K_2 are 480.89 and 1201.14 (band 11), respectively.

Surface emissivity was considered in the estimation of T_s for the LULC targets (El-Magd et al., 2016). The LST (T_s) is estimated using the algorithm in equation 5.

$$T_S = \frac{T_b}{1 + \left(\lambda * \frac{T_b}{\rho}\right) \ln \varepsilon} \tag{5}$$

Where, T_b is the effective satellite temperature, T_s is the absolute LST in Kelvin, λ is the wavelength of the radiance emitted (λ = 11.5μm), ρ = (h × c) / σ = 1.438 ×10^{-2} (m K), h is Planck's constant (6.626 × 10^{-34} Js), c is the velocity of light (2.998 × 10^{8} m/s), σ is the Boltzmann constant (1.38 ×10^{-23} J/K), and ε is the composite emissivity. In this study, ε = 0.95 was used for the soil and vegetation (27). The operations were performed in ERDAS Imagine 13, ENVI Band Math and the ArcMap Raster calculator functions in ArcToolbox (Butt et al., 2015).

4. Results Discussions and Conclusion

4.1 Results of LULC Accuracy Assessment

The Kappa statistic is generally accepted as a measure of classification accuracy for both the model as well as user of the model of classification (35). Kappa values are characterized as <0 as indicative of no agreements and 0–0.2 as slight, 0.2–0.41 as fair, 0.41–0.60 as moderate, 0.60–0.80 as substantial and 0.81–1.0 as almost perfect agreement (Kepner et al., 2000; Chander and Markham, 2003). The overall classification accuracy of the images yielded substantial high *Kappa* statistics of 58%, 72.41% and 82.76% for the 2002, 2008 and the 2014 images, respectively. This is an indication of classification accuracy of moderately substantial to almost perfect agreement (Chander and Markham, 2003).

4.2. Results from 2002 LULC and LST analyses

The LULC class of 2002, as indicated by Figure 4, was an increase over the previous year (1986). In 1986, the LULC categories were 5834 ha, 9181 ha, 1201 ha, 12,722 ha, and 3494 ha for DF, LF, BBC, RFG and WB respectively. These served as the base year of analysis, in terms of vegetated land area coverage. In 2002, dense forest cover was 8760.9 ha of the land cover. A proportion of 30% of the land area was covered by low forest vegetation with 9329.8 ha. The built-up/bare land and concrete surfaces also covered an area of 5664.2 ha. The recent fallows and grassland were reduced to 4422.9 ha of the land area, while the lake covered an area of approximately 3434.9 ha of the total land area.

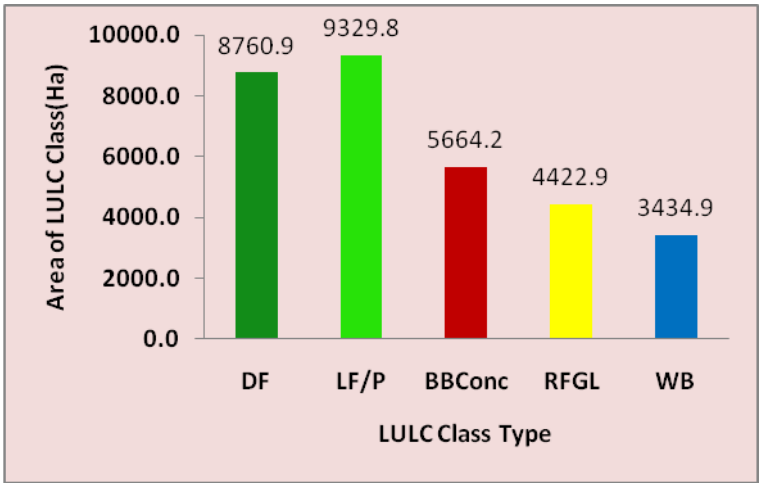

Figure 4: *The area of LULC (ha) for 2002*

The corresponding surface temperature ranged from a minimum of 24ºC (297K) to a maximum of 30ºC (303K), with the mean and standard deviation at 36ºC (308.5K) and 9K respectively. The surface temperature profile indicated an improved vegetated surface which had relatively reduced the surface heat fluxes, thereby, reducing the land surface temperature (Figure 5). This is *in tandem* with Coll et al. (2010)'s assertion that NDVI variables usually negatively correlate with the land surface temperature.

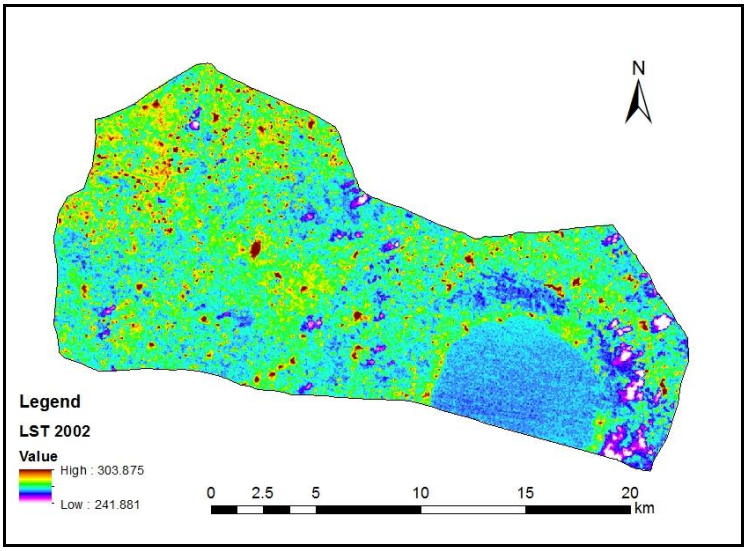

Figure 5: *The 2002 LST extracts showing the surface temperature fluxes*

4.3 Results from 2008 LULC and LST analyses

The land use classes for 2007 showed considerable increase in the DF cover constituting 10,299.9 ha of the total LULC classes in the area. The next cover in order of importance was RFG, which covered an area of 8434.9 ha. BBC surfaces ranked next in terms of coverage with 5451.2 ha. LF was next in terms of coverage importance with 5193.6 ha of the land area (Figure 6). An appreciable proportion of RFG was derived from the exposure of the land surfaces to agriculture and other modes of vegetation removal around the fringes of Lake Bosomtwe (Figure 7). A corresponding surface emission and reflectance translated into LST values ranging between 24ºC (297K) to 53ºC (326K). The mean temperature value was 38ºC (311.5K) and a standard deviation of 20.5K. This result explains; a relatively more rural than urban land use dynamics in the district. The rather high LST anomaly, however, was ostensibly due to the isolated patches of burnt-up surfaces emitting higher heat energy fluxes; in accordance of Stephan-Boltzmann law of surface emissivity (Irish et al., 2006). On the basis of this, the aggregate surface temperature values extracted from the 2008 satellite image gave credence to the rather higher aggregate surface maximum temperature values recorded than the aggregate maximum temperature recorded over the 2014 satellite image; even though, the latter year's built-up and paved surfaces were relatively higher than the former.

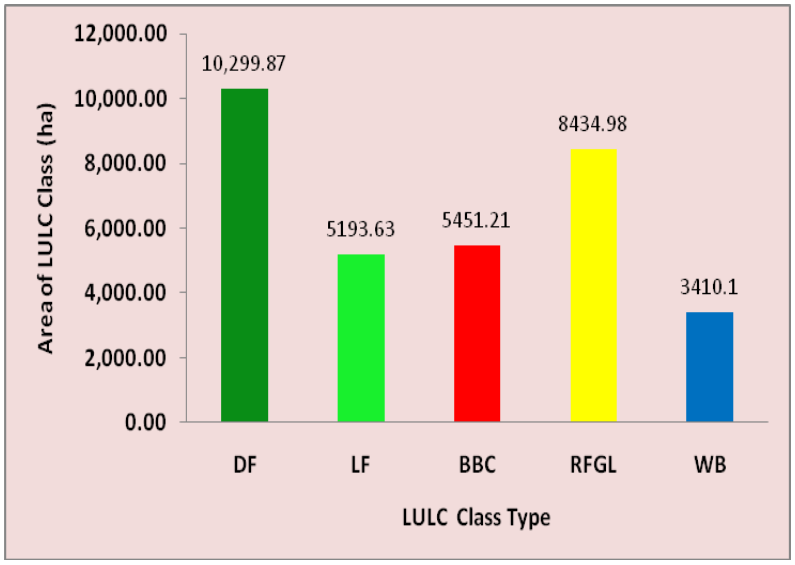

Figure 6: *The Area of LULC (ha) for 2008*

The temperature characteristics were in response to the surface vegetation removal. As human populations increase over time, the demand for land for residential and commercial uses other than forest and agriculture, dominates the landscape. Consequently, the surface becomes exposed to various degrees of heat energy fluxes from insolation with land surface features interactions (Jiménez-Muñoz, and Sobrino, 2013). The surface reflectance characteristics of the land use types, determine, to a greater extent the surface temperature profiles in accordance of the land surface emissivity and reflective capacities. This finding conforms to the result of Rozenstein et al. (2014), who studied global LST for the year for 2013, using at sensor brightness proxy, derived from Landsat with ASTER and AMSR-2 images.

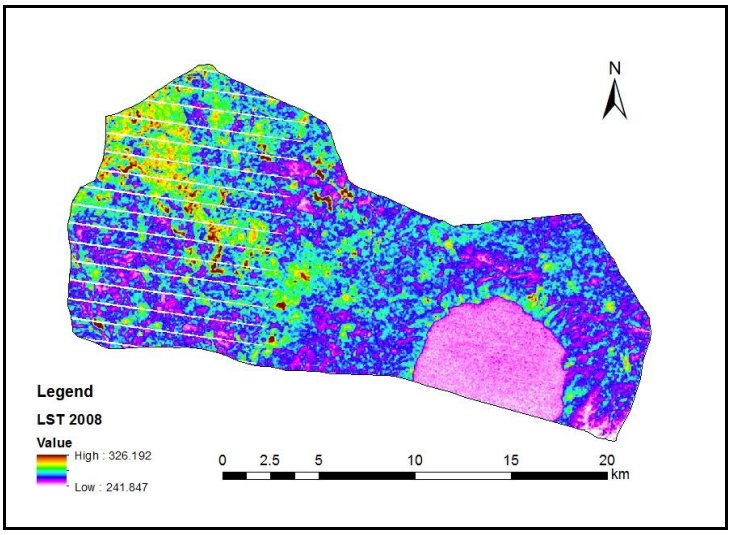

Figure 7: *2008 LST extracts showing the surface temperature fluxes*

4.4 Results from 2014 LULC and LST analyses

The 2014 image shows that the Bosomtwe district had experienced appreciable levels of land cover changes in terms of increasing BBC surfaces (Tursilowati et al., 2012). The LULC classes showed some startling revelation as far as the area coverage of the respective land uses was concerned (Baylis et al., 1999). Invariably, the BBC areas had increased with time up to the year 2014; this is evident by the many PuHT temperature profile, indicated by consistent peaking of the LST graphic for the 2014.

According to Appiah et al. (2015), in a similar work conducted in the study area, low forest cover maintained a high area of coverage with 10,947.83 ha of the total LULC. Recent fallows and grasslands were also next by area of coverage with 9366.75 ha. BBC surfaces, although showed an increase from observation, the statistics of 4596.93 ha by area coverage, indicated an apparent decrease in area from the 2010 image with 5454 ha; representing 14% of the total land area (Appiah et al. (2015). The area covered by the lake, WB, was 3424 ha of the total area (Figure 8).

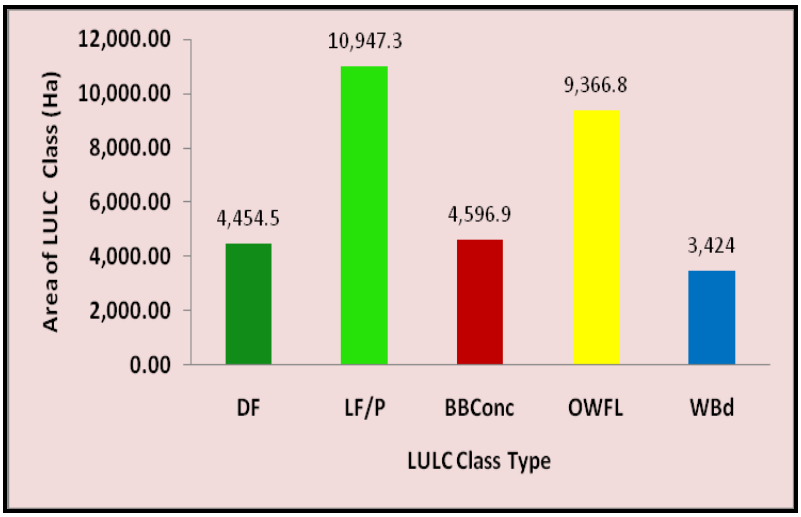

Figure 8: *The Area of LULC (ha) for 2014*

However, the classification scheme that included bare lands as part of the BBC areas resulted in a slower rate of increase in the BBC land uses, as certain parts of the bare lands were re-vegetated. In reality, therefore, the BBC land use type had been increasing with time. Field observations and other auxiliary statistical data, to support this claim for instance, showed increasing trends. Auxiliary data such as the number of houses recorded under the periods by the Ghana Statistical Services Population and Housing Census in 2010 has amply supported the fact that new residential houses increased from 12,399 to 15,525 between the years 2000 and 2010 (Tursilowati et al., 2012). This is indicative of increasing land surface temperature, associated, invariably, with increasing impervious surfaces (Yuan and Bauer, 2007). This was further evidenced by the relatively high LST of 37ºC (310 K) as compared to the minimum of 24 (297K).

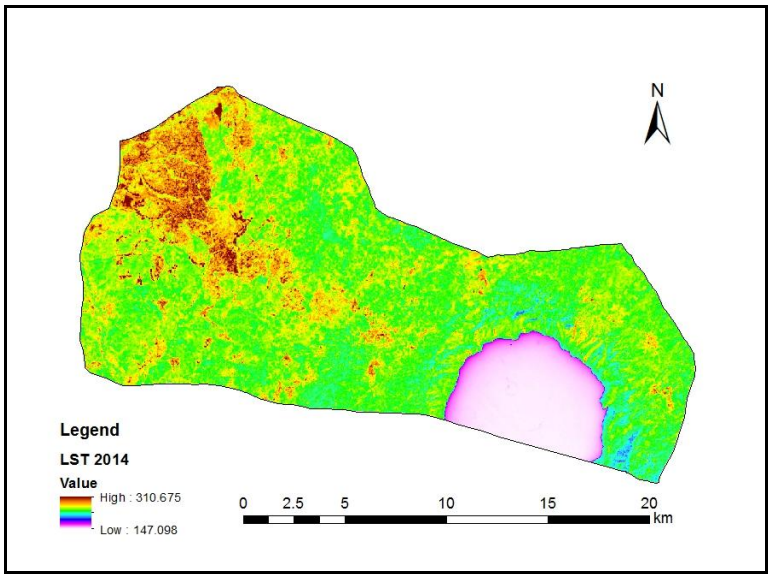

Figure 9: *2014 LST extracts showing the surface temperature fluxes*

The aggregated temperature values from the satellite image land surface temperature extractions are displayed in Figure 10 and Table 2. As indicated in the Figure 10, intermittent occurrences of peri-urban land uses create the heating troughs intervening the rural areas extending from east to west on the map area.

The changing LULC dynamics in the study area over the period under review indicated that there is a correlation between the land use conversion and modifications from one use type to another. As the LULC type changes, its corresponding surface energy emittance is reflected in the recording of the surface sensible heat. Certainly, the 2014 and the 2008 LST graphs depict the surface heat energy amplitude over the entire district, with the peaks indicating isolated pockets of PuHT, measured over the BBC areas. Usually, whenever the rural green and vegetated landscapes become converted into residential and other BBC uses, their surface energy fluxes are changed, and represented by the PuHT, which serves as the intervening energy flux between the RuCT and the ultimate fully-formed UHI; which is a future condition, using the business as usual LULC dynamics in the Bosomtwe district.

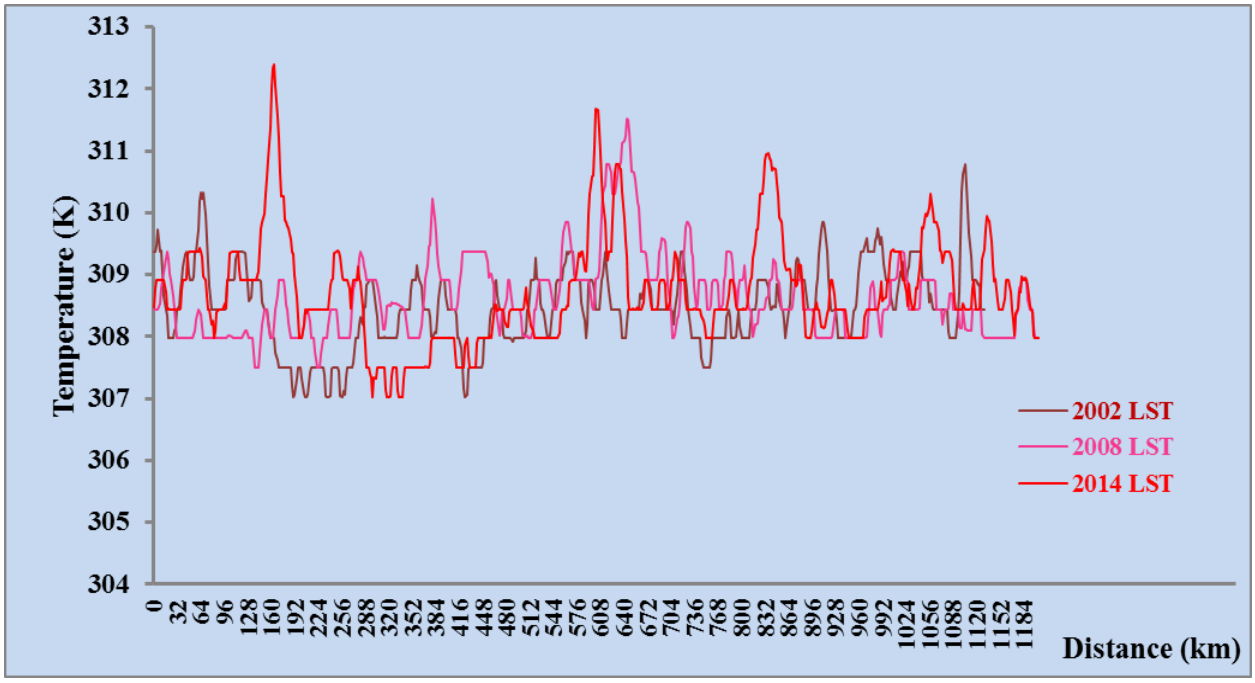

Figure 10: *The composite LST extracts for 2002, 2008 and 2014 showing the PuHT and RuCT areas*

Table 2: *Extracted Maximum, Minimum, Mean and Standard Deviation of Land Surface Temperature from Images*

Satellite Years	Max ºC (K)	Min ºC (K)	Mean ºC (K)
2002	30 (303)	24 (297)	27 (300)
2008	53 (326)	24 (297)	38 (312)
2014	37 (310)	24 (297)	31 (304)

The 12-year duration (2002-2014) also corresponded with an increase in the non-vegetative land uses; particularly, smallholding agriculture land for food crops production. The BBC as well as RFG, in comparison to the vegetated lands, such as the DF and LF covers, which also included some oil palm and citrus fruits plantations, actually increased. The composite statistics of LULC in terms of area in hectares is displayed in Figure 11.

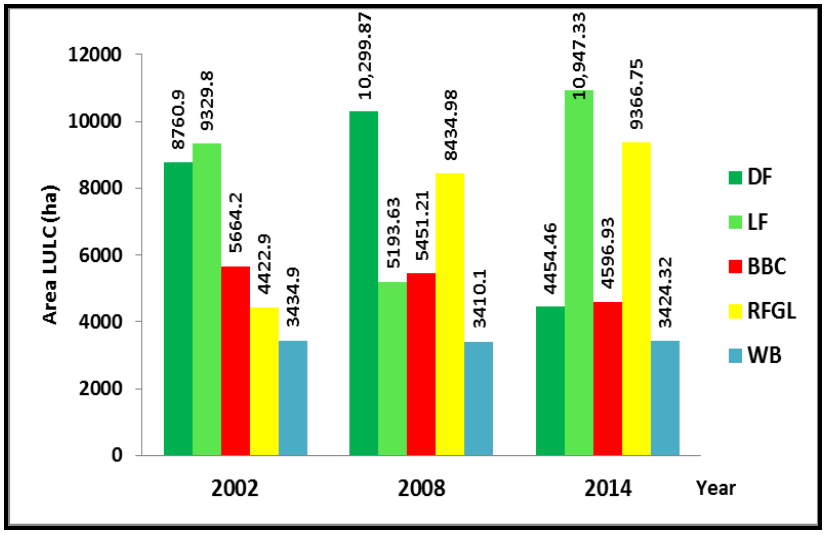

Figure 11: *Grouped bar graph of LULC area statistics in hectares*

4.5 Implications of LULC change on rural and peri-urban LST regimes

The LST regimes invariably corresponded with the LULC types, classified from the satellite images (2a—c). Areas with BBC land uses showed high emittance and reflectance for the records of high temperature profiles. These areas, according to Joshi and Bhatt (2011), are the causes of urban islands in highly dense built urban environments. In rural environments, however, the surface temperature characteristics were observed to be low in comparison to the urban areas. This observation was corroborated by (Ambinakudige, 2012) in a study of Bangalore, India, that anthropogenic activities alter the land cover and expose it to intense heating; thereby causing differential temperature regimes between the urban core and the rural outgrowth areas. The Bosomtwe district also demonstrates similar rural to urban temperature profile. By implication, as rural land uses are replaced by peri-urban BBC surfaces, they eventually become the potential driving forces of PuHT, with the tendencies to generate UHI conditions.

In this context, these PuHT conditions have higher likelihood of occurring in the fast-growing peri-urban towns in the district. Areas such as *Esereso, Jachie, Aputuogya, Kuntenase and Pramso* as shown in Figures 1 & 9, are likely to be influenced by their local micro-climates; and these are likely a function of the land use change dynamics. In the context of this study, an operational and postulated temperature threshold for the PuHT and RuCT in a tropical semi-deciduous climate zone, such as the Bosomtwe district was averaged at 31ºC (303K), which is 1ºC below the district's annual average.

The resultant effects of the changing temperature regime could be expressed in terms of reduced rainfall and increased temperature patterns for an area (Voogt and Oke, 2003). If this trend of LULC change continues into the future, a drastic near to full UHI is imminent in the rapidly urbanizing peri-urban fringes, considering business as usual scenarios. For replication, the temperature threshold values could be calibrated based on the type of climatic region under consideration. The associated land surface emissions from the various LULC types yielded corresponding LSTs, in consonance with a similar work by Kumar et al. (2016). This phenomenon, presents an opportunity for the formation of PuHT. When juxtaposed with the RuCT, there is the tendency for surface energy fluxes dissipation from the rural areas with high vegetation cover, to serve as carbon sinks that can regulate local surface warming effects (LSWE) (Maingi and Marsh, 2002; Boori et al., 2015).

The study has buttressed the fact that there exists a correlation between LULC emissivity and surface temperature profiles. These have tendencies to support the PuHT and RuCT concepts, proposed and espoused in this paper. The land surface configurations and their attendant variability in terms of temperature, suggest that the use of NDVI may not be an adequate measure of quantifying surface heat island (SUHI) systems; but with the addition of other approaches, this is reliable (Coll et al., 2010), (Ogashawara and Da Silva Brum Bastos, 2012), (Bhatt et al., 2013). To address this anomaly, Weng et al. (2004) postulated the use of vegetation fraction identified within a pixel. This is derived from a spectral combination of different LULC fragments, instead of solely relying on NDVI as a metric indicator. Their findings showed that vegetation fraction showed a moderate relationship with LST Appiah et al. (2015); Li et al. (2011) which coheres amply with the situation in the Bosomtwe district of Ghana.

4.6 Conclusion and Recommendation

This paper argued that, the transition from a rural to an urban area also exhibits a temperature profile that traverses through a RuCT through a PuHT, respectively, before achieving the ultimate UHI condition. The results obtained from the analyses of the LULC and the LST maps, have some land use and climate variability policy implications. The paper espouses that the land use pattern, in the Bosomtwe district's is changing from rural to peri-urban, through the replacement of the arable farm

lands and forest covers with built up concrete infrastructure. This observation, therefore, supports the PuHT and RuCT conditions that result from changing rural and peri-urban landscape configuration, as proposed by this study.

The land surface characteristics and their associated LST variability, suggest that the Bosomtwe district, a hitherto predominantly rural area is gradually becoming peri-urbanized. To address this anomaly, the implementation of the peri-urban land use policy framework of the Bosomtwe district assembly should be strictly enforced, where necessary. This would ensure that land uses that do not, as a matter of urgency require land use conversions from their original land use types such as forest covers and arable agricultural lands, would be preserved, to enhance surface cooling.

It is also proffered that in order to curtail the rapid development of PuHT systems, which are the fuelling cells of the UHIs; there is the need for the implementation of peri-urban greening and land use modification policy strategies. The implementation of these measures would serve as a mitigation measures that would preserve most of the rural landscape configuration, which would enhance more RuCT systems rather than the PuHTs that could adversely affect the local micro-climatic sub-system, with possible regional consequences on agriculture and other livelihood activities in the district.

A further investigation and the determination of an average temperature value as a threshold for the measurement of the RuCT and PuHT in tropical sub-humid climatic zones, where the study district is located is proffered, for further research.

Disclosures

All authors declare no conflict of interest in this paper.

Acknowledgement

The authors are grateful to the German Federal Ministry of Education (GMBF) through the West African Science and Service Centre of Climate Change and Adapted Land Use, for the financial support in the form of a scholarship for this study. We also thank the Department of Photogrammetry and Geoinformatics, Stuttgart University of Applied Sciences immensely, for the use of their Remote Sensing and GIS laboratory to get access to the current software for this study. We thank Ms Jemimah Abena Nyamekye and Patricia Aidoo for their proof-reading of the manuscript for the language and grammatical coherence. We finally thank the anonymous reviewers for their constructive critique of the paper.

References

Ahrens, C.D. 2005. *Essentials of Meteorology: An introduction to the Atmosphere*, 4th Edition, Belmont, USA: Thompson/Brooks/Cole, p.473.

Ambinakudige, S. 2011. Remote sensing of land cover's effect on surface temperatures: a case study of the urban heat island in Bangalore, India*. Applied Geographic Information System*, 7(1), pp.1-12.

Appiah, D.O., Adanu, S.K., Forkuo, E.K. and Bugri, J.T. 2015. Normalized Difference Vegetation Index Analysis of the Vegetation Cover in Bosomtwe Peri-Urban Settlement, Ghana*. Journal of Basic and Applied Research International*, 5(3), pp.146-156.

Appiah, D.O., Bugri, J.T. and Forkuo E.K. 2015. Modelling the Perspective of Agricultural Land Use Trajectories in a Peri-Urban District of Ghana. *Journal of Scientific Research & Reports*, 5(1), pp.16-31.

Appiah, D.O., Schroeder, D., Forkuo E.K. and Bugri, J.T. 2015. Application of Geo-Information Techniques in Land Use and Land Cover Change Analysis in a Peri-Urban District of Ghana. *International Journal of Geo-Information*, 4, pp.1265-1289.

Asmat, A., Mansor, S., Saadatkhah, N., Adnan, N.A. and Khuzaimah, Z. 2016. Land Use Change Effects on Extreme Flood in the Kelantan Basin Using Hydrological Model. Springer, ISFRAM, pp.221-236. DOI: 10.1007/978-981-10-0500-8_18.

Baylis, M., Meiswinkel, R. and Venter, G.J. 1999. A preliminary attempt to use climate data and satellite imagery to model the abundance and distribution of Culicoides imicola (Diptera: Ceratopogonidae) in Southern Africa. *Journal of the South African Veterinary Association*, 70(2), pp.80-89.

Bhatt, U.S., Walker, D.A., Raynolds, M.K., Bieniek, P.A., Epstein, H.E., Comiso, J.C., Pinzon, J.E., Tucker, C.J. and Polyakov, I.V. 2013. Recent Declines in Warming and Vegetation Greening Trends over Pan-Arctic Tundra. *Remote Sensing*, 5, pp.4229-4254.

Blake, R., Grimm, A., Ichinose, T., Horton, R., Gaffin, S., Jiong, S., Bader, D., and Cecil, L.D. nd. *Urban climate: Processes, trends, and projections. Climate Change and Cities: First Assessment Report of the Urban Climate Change Research Network*, In: C. Rosenzweig, W.D. Solecki, S.A. Hammer, S. Mehrotra (eds.), Cambridge, UK: Cambridge University Press, pp.43-81.

Bonan, G.B., Oleson, K.W. and Vertenstein, M. 2002. The land surface climatology of the community land model coupled to the NCAR community climate model. *Journal of Climatology*, 15, pp.3123-3149.

Boori, M.S., Balzter, H., Choudhary, K. Kovelskiy, V. and Vozenilek, V. 2015. *A Comparison of Land Surface Temperature, Derived from AMSR-2, Landsat and ASTER Satellite Data. Journal of Geography and Geology*, 7(3), 61-69.

Butt, A., Shabbir, R., Ahmad, S.S. and Aziz, N. 2015. Land use change mapping and analysis using Remote Sensing and GIS: A case study of Simly watershed, Islamabad, Pakistan. *The Egyptian Journal of Remote Sensing and Space Sciences*, 18, pp.251-259.

Carnahan, W.H. and Larson, R.C. 1990. An analysis of an urban heat sink. *Remote Sensing of Environment*, 33, pp.65-71.

Chander, G. and Markham, B. 2003. Revised Landsat-5 TM Radiometric Calibration Procedures and Post-calibration Dynamic Ranges. *IEEE Transactions on Geoscience and Remote Sensing*, 41(11), pp.2674-2677.

Chen, X-L., Zhao, H-M., Li, P-X. and Yin, Z-Y. 2006. Remote sensing image-based analysis of the relationship between urban heat island and land use/cover changes. *Remote Sensing of Environment*, 104, pp.133-146.

Coll, C. Galve, J.M., Sánchez, J.M. and Caselles, V. 2010. Validation of Landsat-7/ETM+ Thermal-Band Calibration and Atmospheric Correction with Ground-Based Measurements. *IEEE Transactions on Geoscience and Remote Sensing,* 48(1), pp.547-555.

Coll, C., Caselles, V. and Galve, J.M. 2005. Ground measurements for the validation of land surface temperatures derived from AATSR and MODIS data. *Remote Sensing of Environment*, 97, pp.288-300.

Cristobal, J., Jimenez-Munoz, J.C., Sobrino, J.A., Ninyerola, M. and Pons, X. 2009. Improvements in land surface temperature retrieval from the Landsat series thermal band using water vapor and air temperature. *Journal of Geophysical Research*, 114, pp.841-846, doi: 10.1029/2008JD010616.

Dousset, B. and Gourmelon, F. 2003. Satellite multi-sensor data analysis of urban surface temperatures and land cover. *Photogrammetry and Remote Sensing*, 58, pp.43-54.

ElMagd, I.A., Ismail, A. and Zanaty, N. 2016. Spatial Variability of Urban Heat Islands in Cairo City, Egypt using Time Series of Landsat Satellite Images. *International Journal of Advanced Remote Sensing and GIS*, 5, pp.1618-1638. doi:10.23953/cloud.ijarsg.48

Iino, A. and Hoyano, A. 1996. Development of a method to predict the heat island potential using remote sensing and GIS data. *Energy Building*, 23, pp.199-205.

Irish, R.R., Barker, J.L., Goward, S.N. and Arvidson, T. 2006. Characterization of the Landsat-7 ETM Automated Cloud-Cover Assessment (ACCA) Algorithm. *Photogrammetric Engineering and Remote Sensing*, 72(10), pp.1179-1188.

Jiménez-Muñoz, J.C, Sobrino, J.A., Gillespie, A., Sabol, D. and Gustafson, W.T. 2006. Improved land surface emissivities over agricultural areas using ASTER NDVI. *Remote Sensing of Environment*, 103, pp.474-487.

Jiménez-Muñoz, J.C. and Sobrino, J.A. 2013. A generalized single-channel method for retrieving land surface temperature from remote sensing data. *Journal of Geophysical Research*, 108(D22), pp.1-9.

Joshi, J.P. and Bhatt, B. 2012. Estimating temporal land surface temperature using remote sensing: a study of Vadodara urban area, Gujarat. *International Journal of Geology, Earth and Environmental Sciences,* 2(1), pp.123-130.

Kepner, W.G., Watts, C.J., Edmonds, C.M., Maingi, J.K., Marsh, S.E. and Luna, G. 2000. A Landscape Approach for Detecting and Evaluating Change in a Semi-arid Environment. *Environmental Monitoring and Assessment*, 64(1), pp.179-195.

Khang, Y., Khan, S. and Ma, X. 2009. Climate change impacts on crop yield, crop water productivity and food security– A review. *Progress in Natural Science*, 19(12), pp.1665-1674.

Kumar, S.K., Bhaskar, P.U. and Kumari, K.P. 2016. Emerging Urban Heat Islands in the New Capital Region of Andhra Pradesh, India - A Satellite based Evaluation. *International Journal of Advanced Remote Sensing and GIS*, 5, pp.1915-1929. doi:10.23953/cloud.ijarsg.69

Li, J., Song, C., Cao, L., Zhu, F., Meng, X. and Wu, J. 2011. Impacts of landscape structure on surface urban heat islands: A case study of Shanghai, China. *Remote Sensing of Environment*, 115, pp.3249-3263.

Lipton, A.E. and Ward, J.M. 1997. Satellite-view biases in retrieved surface temperatures in mountain areas. *Remote Sensing of Environment*, 60, pp.92-100.

Liu, L. and Zhang, Y. 2011. *Urban Heat Island Analysis Using the Landsat TM Data and ASTER Data: A Case Study in Hong Kong*. Remote Sensing, 3, 1535-1552.

Maingi, J.K. and Marsh, S.E. 2002. An Accuracy Assessment of 1992 Landsat-MSS Derived Land cover for the Upper San Pedro Watershed (U.S./Mexico); United States Environmental Protection Agency: Washington, DC, USA, 2002; 29p.

Mbithi, D.M., Demessie, E.T. and Kashiri, T. nd. The impact of Land Use Land Cover (LULC) changes on Land Surface Temperature (LST); a case study of Addis Ababa City, Ethiopia. Kenya Meteorological Services, Laikipia Airbase, Kenya, 8pp.

Meehl, G.A., Stocker, T.F. and Collins, W.D. 2007. Global climate projections. In: Solomon, S., Qin, D., Manning, M., et al., (eds.), *Climate change 2007: the physical science basis*. *Contribution of working group I to the fourth assessment report of the intergovernmental panel on climate change.* Cambridge: Cambridge University Press, p.749-844.

Mousivand, A., Verhoef, W., Menenti, M. and Gorte, B. 2015. Modelling top of atmosphere Radiance over Heterogeneous Non-Lambertian Rugged Terrain. *Remote Sensing*. 2015. 7, pp.8019-8044.

Ogashawara, I. and Da Silva Brum Bastos, V.A. 2012. Quantitative Approach for Analyzing the Relationship between Urban Heat Islands and Land Cover. *Remote Sensing*, 4, pp.3596-3618.

Quattrochi, D.A., Luvall, J.C., Rickman, D.L., Estes Jr., M.G., Laymon, C.A. and Howell, B.F. 2000. A decision support information system for urban landscape management using thermal infrared data. *Photogrammetric Engineering and Remote Sensing*, 66, pp.1195-1207.

Rajeshwari, A. and Mani, N.D. 2014. Estimation of land surface temperature of Dindigul District using Landsat 8 data. *International Journal of Research in Engineering and Technology*, 3(5), pp.122-126.

Rozenstein, O., Qin, Z., Derimian Y. and Karnieli, A. 2014. Derivation of Land Surface Temperature for Landsat-8 TIRS Using a Split Window Algorithm. *Sensors*, 14, pp.5768-5780.

Sobrino, J.A., El Kharraz, J. and Li, Z-L. 2003. Surface temperature and water vapour retrieval from MODIS data. *International Journal of Remote Sensing*, 24, pp.5161-5182.

Sobrino, J.A., Jiménez-Muñoz, J.C. and Paolini, L. 2004. Land surface temperature retrieval from LANDSAT TM 5. *Remote Sensing of Environment*, 90, pp.434-440.

Srivastava, P.K., Majumdar, T.J. and Bhattacharya, A.K. 2010. *Study of land surface temperature and spectral emissivity using multi-sensor satellite data*. *Journal of Earth System Sciences*, 119(1), pp.67-74.

Thomas, A. 2008. Agricultural irrigation demand under present and future climate scenarios in China. *Global Planetary Change*, 60, pp.306-326.

Tursilowati, L., Sri Sumantyo, J.T., Kuze, H. and Sri Adiningsih, E. 2012. Relationship between Urban Heat Island Phenomenon and Land Use/Land Cover Changes in Jakarta-Indonesia. *Journal of Emerging Trends in Engineering and Applied Sciences*, 3(4), pp.645-653.

Urban, A., Davídkovov, H. and Kysley, J. 2013. Heat- and cold-stress effects on cardiovascular mortality and morbidity among urban and rural populations in the Czech Republic. *International Journal of Biometeorology,* 58(6), pp.1057-1068.

USGS. 2015. Using the USGS Landsat 8 Product. Accessed on 28 January 2016 at http://landsat.usgs.gov/Landsat8_Using_Product.php

Vlassova, L., Pérez-Cabello, F., Mimbrero, M.R., Llovería, R.M. and García-Martín, A. 2014. Analysis of the Relationship between Land Surface Temperature and Wildfire Severity in a Series of Landsat Images. *Remote Sensing*, 6, pp.6136-6162.

Voogt, J.A. and Oke, T.R. 2003. Thermal remote sensing of urban climates. *Remote Sensing of Environment,* 86, pp.370-384.

Weng, Q. 2001. A remote sensing–GIS evaluation of urban expansion and its impact on surface temperature in the Zhujiang Delta, China. *International Journal of Remote Sensing*, 22(10), 1999-2014.

Weng, Q., Lu, D. and Schubring, J. 2004. Estimation of land surface temperature–vegetation abundance relationship for urban heat island studies. *Remote Sensing of Environment*, 89, pp.467-483.

Widyasamratri, H., Souma, K., Suetsugi T., Ishidaira H., Ichikawa Y., Kobayashi H. and Inagaki I. 2013. *Air Temperature Estimation from Satellite Remote Sensing to Detect the Effect of Urbanization in Jakarta, Indonesia*. *Journal of Emerging Trends in Engineering and Applied Sciences*, 4(6), pp.800-805.

Yuan, F. and Bauer, M.E. 2007. Comparison of impervious surface area and normalized difference vegetation index as indicators of surface urban heat island effects in Landsat imagery. *Remote Sensing of Environment,* 106, pp.375-386.